بسم الله الرحمن الرحيم

Sudan University of Science and Technology

College of Graduate Studies

Study of the Luminescent Properties of Cerium Ion Doped Mixed Fluoride Materials

دراسة الخواص الضوئية لايون السيريوم المشوب في خليط من مواد الفلورايد

A thesis submitted to complete requirements of a MSc degree in physics science

Prepared by

Safa Osman Daowd Omer

Supervisor: Dr. Mubarak Yagoub

March/2020

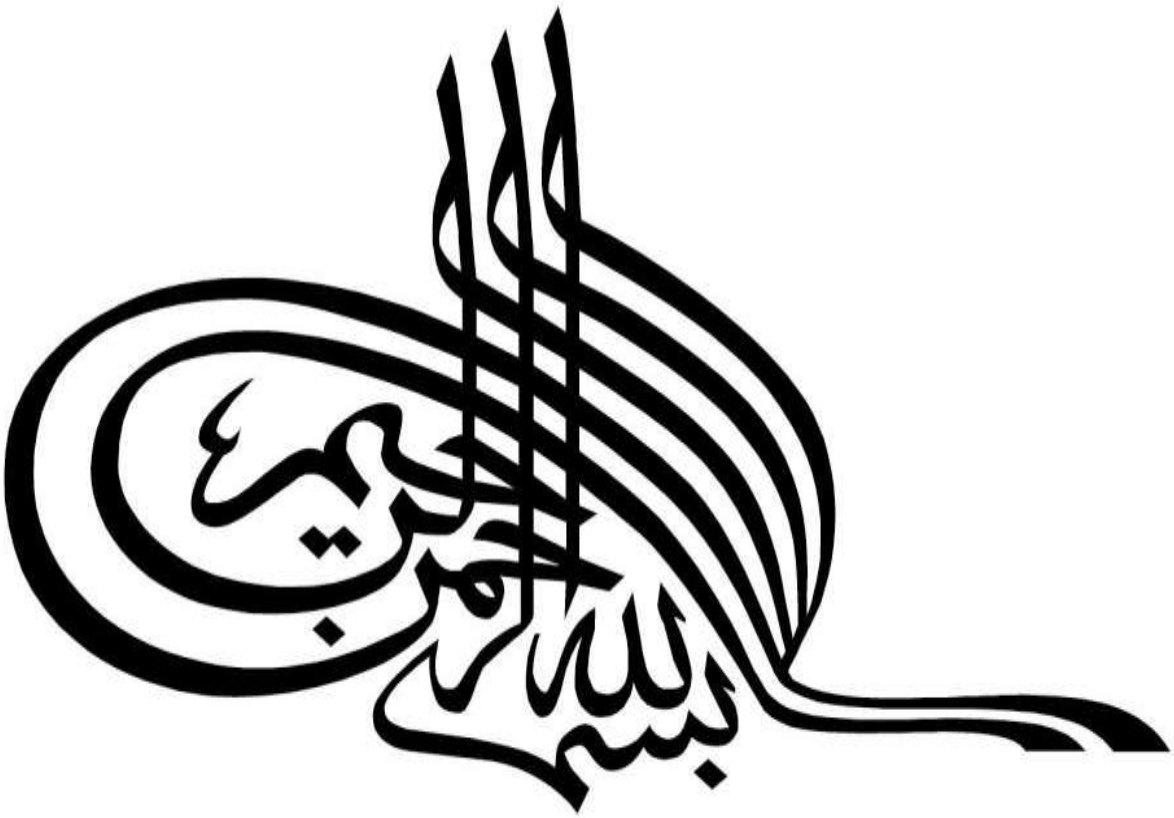
بسم الله الرحمن الرحيم

الايـــــة

قال تعالى:-

(قَالُوا سُبْحَانَكَ لَا عِلْمَ لَنَا إِلَّا مَا عَلَّمْتَنَا إِنَّكَ أَنْتَ الْعَلِيمُ الْحَكِيمُ)

سورة البقرة الآية(32)

Dedication

I dedicate this thesis to

Those whose tired fingertips give us a moment of happiness

Those who harvested thorns from my path to facilitate my path of

those who drank the cup empty to give me love

Knowledge

The Big Heart (my dear father)

those who have placated me with love and affection

The symbol of love and healing balm

The white heart (my dear mother)

The kind, pure souls of the winds of my life (my sisters) and the second half of my life (my friends)

ACKNOWLEDGMENT

Thanks for everyone who stood on the pulpits and gave from the outcome of his thought to enlighten our path We especially thank and gratitude Dr. Mubarak Yagoub, who preferred to supervise this research, may God reward him My respect is highly appreciated and respected

ABSTRACT

The purpose of this study was to analyze the structural properties of fluoride materials mixed with cesium and to study the photoluminescence of cesium and the effect of the mixture on the photoluminescence of cesium.

Investigations were done to modify the photoluminescence (PL) spectra of a cerium doped mixed fluoride of $Sr_{0.49}M_{0.5}Ce_{0.01}F_2$ (where M = Ca, Ba, Mg) materials. The x-ray diffraction analysis revealed that the Fm3m space group unchanged by substitution Sr atom by alkali earth fluorides. A noticeable shift in the x-ray diffraction patterns is observed in all ions substitution. The investigation of the photoluminescent behavior of Ce3+ in $Sr_{0.49}M_{0.5}Ce_{0.01}F_2$ showed noticeable change in the shape of the excitation and emission spectra of Ce3+. The Sr0.49Ba0.50Ce0.01F2 materail produced a significant red shift with a broad emission band. The excitation spectrum of this sample was blue shifted and therefore not suitable for solar cell application.

لمستخلص

هدفت هذه الدراسة إلى تحليل الخصائص التركيبية لمواد الفلورايد الخليط المشوب مع السيريوم ودراسة اللمعان الضوئي للسيريوم وأثر الخليط على اللمعان الضوئي للسيريوم. أجريت التحقيقات لتعديل أطياف التلالؤ PLلفلورايد الخليط مشوب من السيريوم من المواد $Sr_{0.49}M_{0.5}Ce_{0.01}F_2$ حيث(Mg) M = Ca, Ba and . كشف تحليل حيود الأشعة السينية أن المجموعة الفضائية. لم تتغير باستبدال ذرة بفلورايد الأرض القلوية. لوحظ تحول ملحوظ في أنماط حيود الأشعة السينية في استبدال جميع الايونات. أظهر التحقيق في سلوك الإضاءة الضوئية ل$Sr_{0.49}M_{0.5}Ce_{0.01}F_2$ تغير ملحوظ في شكل الإثارة و أطياف الانبعاث لCe^{3+} . أنتجت مادة$Sr_{0.49}Ba_{0.5}Ce_{0.01}F_2$ تحولا أحمر كبير في نطاق انبعاث عريض. تم إزاحة طيف الإثارة لهذه العينة باللون الأزرق وبالتالي لم يكن مناسبا للتطبيق في الخلايا الشمسية.

.

Index

List of Figure

CHAPTER ONE

INTRODUCTION

1.1 General Overview

Luminescence is a phenomenon of emitting light upon excitation with different excitation forms. When the source of excitation is photon the phenomenon called photoluminescence (PL). In semiconductor materials, an energy of incident photon that equal or beyond the energy band gap can excite electron from valance band into conduction band. This process also known as absorption. The absorption can also happen when an electron is excited to higher energy level from natural acceptor energy level and it can also transit to ionization donor energy level from valance or transit to conduction band from ionization acceptor energy level. The phenomena can explain the energy band or impurities in the semiconductors successfully [1].

According to analytic data of PL we can know the kind of impurities, band gap and impurity activation energy from the spectra. We can estimate the composition of compound from peak intensity of PL spectra. Using photoluminescence can investigated the internal interface of the hetero-structure that general physical or electronic measurements cannot measure [2].

Lanthanide ions possess fascinating optical properties that make them utilized in various applications. The first discovery was their uses in industrial and nowadays high technological application are largely governed by their interaction with light. Lighting devices (economical luminescent lamps, light emitting diodes), television and computer displays, optical fibers, optical amplifiers, lasers, as well as responsive

luminescent stains for biomedical analysis, medical diagnosis, and cell imaging rely heavily on lanthanide ions [3].

The fluoride materials (such as SrF_2, BaF_2 and CaF_2) possess a set of unique physical and luminescent properties. They are practically feasible and can be grown to have sufficient size and optical quality to create optical media. Moreover, they are highly transmitted to most spectra from NIR to UV regions.

Therefore, they can be used in many application when doped with appropriate activators such as lanthanide ions [1].

Cerium ion (Ce^{3+}) is one of the lanthanide ions that his emission strongly depends on the crystal field of the host structure. The emission of Ce^{3+} ion originates from the allowed transition party from 5d level to 4f level unlike other trivalent lanthanide ions that emits through 4f-4f transition. This means one can tune the emission of Ce^{3+} with changing the atoms around the Ce^{3+} ions. For examples, when Ce^{3+} doped SrF_2 emits light in UV region around 330 nm [4]. Whereas Ce^{3+} in CaF_2 gives light in slightly larger wavelength. The emission of Ce^{3+} ion in oxygen legends can be shifted up to NIR region []. This property of Ce^{3+} ion emission makes it utilized in many different application depending on the emission wanted.

One of the most promising application of lanthanide doped fluoride materials is in solar cells. SrF_2 doped with Pr^{3+}-Yb^{3+} ions turned to emit strongly in NIR emission where the absorption efficiency of crystalline solar cell is relatively weak [5]. Despite the promising results but the practical application of SrF_2: Pr^{3+}-Yb^{3+} in solar cell is far. This is due to the low absorption strength of Pr^{3+} ion in visible region due to it is 4f-4f weak absorption strength. The solution was suggested the use one of the Ce^{3+} or Eu^{2+} lanthanide ions as sensitizer to absorbed the UV-blue photon

through their allowed absorption transition and then feed the Pr^{3+}-Yb^{3+} couple [4].

Ce^{3+} in SrF_2 ions absorbs strongly in 250-300 nm range, which is practically cannot be used in solar cell application. Furthermore, the emission of Ce^{3+} doped SrF_2 is far from the excitation region of the most trivalent lanthanide ions [4]. a method of shifting Ce^{3+} absorption and emission to blue region is required and useful in solar cell application.

1.2 Research Problem

As mentioned in above section that the PL of some of the lanthanide ion depends strongly on the crystal field of the host environments. Therefore a region where the lanthanide ions emit determines the corresponding application. Therefore, in this study investigated the structural and luminescence properties of Ce^{3+} doped mixed alkaline earth fluoride materials for possible redshift in its emission.

1.3 Objectives

This research aims to achieve the followings

- Analyze the structural properties of mixed fluoride material of SrMF2:Ce3+ (where M is Ca, Mg and Ba) using x-ray diffraction technique.
- Analyze and identify the photoluminescence of Ce^{3+} ion in mixed fluoride material.
- Study of the effect of mixing fluoride materials on the photoluminescence of Ce^{3+} ion.

1.4 Thesis Layout

This work, consisting of five chapters, this chapter one include, the introduction, which gives general overview and definition of the research problem. In chapter two, the basic concepts that are necessary to understand the background information of this work were briefly discussed. It is followed by a brief description of the experimental

procedures and the techniques that were used in this study, chapter three. Chapter four provides the results and discussion. Conclusion is given in chapter 5.

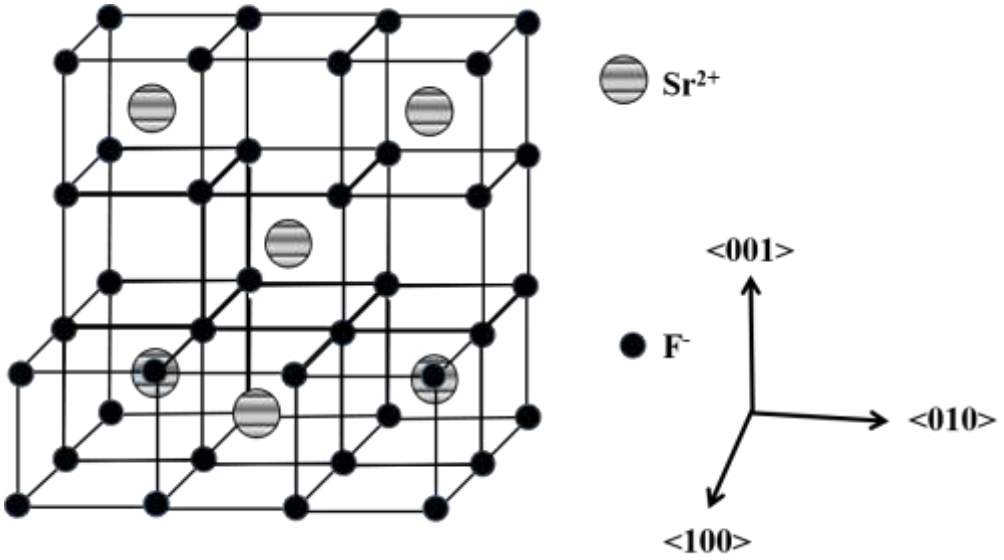

Figure 2.1 : A schematic diagram of the pure SrF_2 structure, which it shows each second simple cubic of F^- sublattic contains an Sr^{2+} ion and the other are empty

The dopant ions are most often Ln^{3+}. The divalent ions (Ln^{2+}) simply substitute Sr^{2+} ions in the crystal to form crystal defects with cubic symmetry. Surprisingly, up to 40% of the Ln^{3+} ions may replace Sr^{2+} lattice leaving the structure without significantly change [8]. When Ln^{3+} ions are doped in SrF_2, the extra positive charge relative to the Sr^{2+} ion makes some type of charge-compensation mechanism necessary, which is required to maintain the electrical neutrality of the crystal. A number of crystal defects (or crystal field effects) can be formed when Ln^{3+} ions are doped in SrF_2, see Fig. 2.2.

CHAPTER TOW

BACKGROUND INFORMATION

2.1 Luminescence

Luminescence is the emission of light from any material and occurs from electronically excited state. Luminescence is formally divided into two categories-fluorescence and phosphorescence depending on the nature of the excited state. Firstly the fluorescence, in exited singlet state the electron in the excited orbital is paired (by the opposite spin) to the second electron in the ground-state orbital. Consequently, return to the ground state is spin allowed and occurs rapidly by emission of a photon. The emission rates of fluorescence are typically 10^8 s^{-1}, so that a typical fluorescence lifetime is near 10 ns ($10*10^{-9}$ s) [6].

Secondly, Phosphorescence is emission of light from triplet excited states, in which the electron in the excited orbital has the same spin orientation as the ground-state electron. Transitions to the ground state are forbidden and the emission rates are slow (10^3 to 10^0 s^{-1}), so that phosphorescence lifetimes are typically milliseconds to seconds. Even longer lifetimes are possible, as is seen from "glow-in-the-dark" toys. Following exposure to light, the phosphorescence substances glow for several minutes while the excited phosphors slowly return to the ground state. Phosphorescence is usually not seen in fluid solutions at room temperature. This is because there exist many deactivation processes that compete with emission, such as non-radiative decay and quenching processes. It should be noted that the distinction between fluorescence and phosphorescence is not always Clear. Transition Metal Ligand complexes (MLCs), which contain a metal and one or more organic

ligands, display mixed singlet– triplet states [6]. These MLCs display intermediate lifetimes of hundreds of nanoseconds to several microseconds.

2.2 Strontium Fluoride (SrF_2) Structure

SrF_2 crystal has attract much attentions from many researchers over the last several decades. SrF_2 is one of the alkaline earth fluorides materials. The alkaline earth fluorides are an important class of materials that form the basis of a range of applications such as geosciences and materials science. In terms of the applications, the alkaline earth fluorides have attracted considerable interest due to their unique properties, including low-energy phonons, high ionicity, electron-acceptor behavior, high resistivity, and anionic conductivity [7]. SrF_2 crystallizes in cubic fluorite structure with a space group of Fm3m, which consists of a cubic close-packed array of cations with anions occupying tetrahedral sites. The structure of SrF_2 has eight fluorine atoms arranged in a cube around the alkaline earth atom, with the cubes of fluorine edge-connected in a face centered cubic array. Conversely, the fluorine atom is surrounded by four Sr^{2+} cation atoms arranged in an ideal tetrahedron with the tetrahedral also edge-connected. It has a face centered cubic (FCC) structure and a space lattice of symmetry O_h [7]. The crystal consists of a simple cubic lattice of F^- anions with Sr^{2+} cations occupying every second cube formed by the F lattice. This results in six interstitial sites or empty cubes surrounding each Sr^{2+} ion (see Fig. 2.1). The existence of vacant cubic sites equal in number to the occupied cation sites enables the SrF_2 crystal to host a large number of anion F interstitials. Among these fluoride crystals is SrF_2. SrF_2 is an ionic crystal with a molecular weight of 125.62 atomic unit and melting temperature of 1477^o C. It has a lattice constant of 5.798 Å [8].

SrF_2 is an insulator and optically transparent. It consists of quite a large band-gap of around 11 eV. Thermal excitation, however, may lead to anion Frenkel defects [8]. This makes SrF_2 a weak ionic conductor at room temperature. The cation Frenkel defects in SrF_2 have large formation energy, therefore, their effect is small. At close to melting temperature, the SrF_2 may undergo a superionic phase transition, where a sudden increase of anion Frenkel defects occurs and the material becomes a superconductor. Basically, the anion sublattice melts whereas the cation lattice remains relatively stable [8]

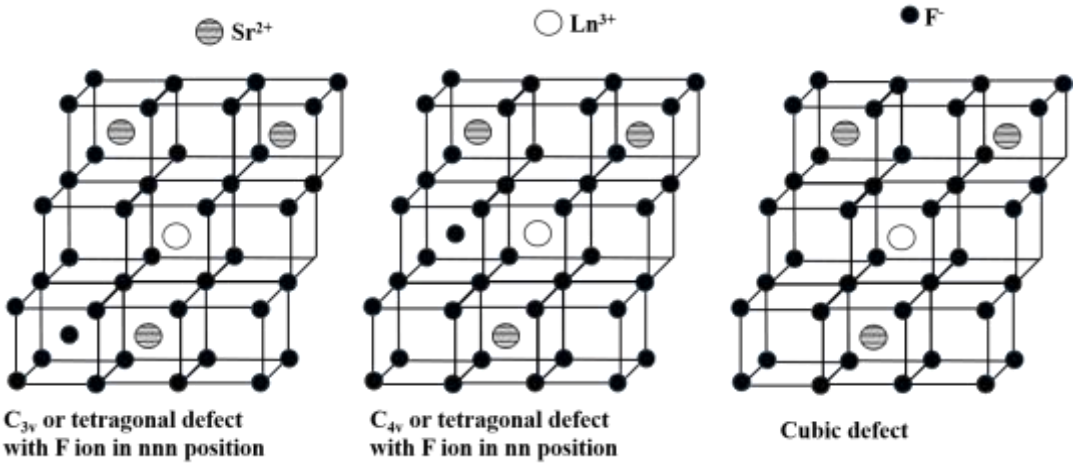

Fig. 2.2: Some common structure defects involving Ln^{3+} ions.

2.3 Lanthanide ions

The rare-earth elements are a homogeneous group of 17 elements. They correspond to elements of atomic number of 57– 71 (La-Lu) in the periodic table. The trivalent form of the lanthanide (Ln^{3+}) ions have electronic configuration of $4f^n5s^25p^6$ where n is the number of electrons (from 0 to 14). The partly allowed 4f level is important in the optical and magnetic properties of the lanthanides. The number of 4f orbital configurations for n electrons is given by (14!=[n!(14-n)!], and each configuration can have a specific energy. The shielding of 4f orbital by the allowed 5s and 5p outer electrons makes the 4f electrons weakly affected by the ligand ions in crystals. As a results the lanthanide 4f-4f

electronic transitions exhibit relatively narrow lines in the luminescence and absorption spectra. Such transitions are forbidden by the Laporte selection rule, which states that \state that with even parity can be connected by electric dipole transitions only with states of odd parity, and odd states only with even ones" [9]. The transitions within the 4f shell are forbidden in term of electric dipole transitions, but allowed for magnetic dipole or electric quadrupole radiation. Although electric dipole transition is forbidden it may occur but with low probability [9].

Dieke et al. [10] studied the energy of the 4f electrons of the Ln^{3+} ions. Their calculation results is shown in a diagram known as the Dieke diagram, shown in Fig. 2.3. Nowadays, it is a common reference that used to estimate the low-lying fn levels of the Ln^{3+} ions. In the Dieke diagram, the thickness of the level indicates the degree of the crystal field splitting and the location of the free ion $^{2s+1}L_J$ approximated from the center of the multiplet level. The energy splitting slightly changes when the Ln^{3+} ions are incorporated into different crystals, but the dominant spectral features remain unchanged [11].

In contrast to 4f orbital, the crystal field in 5d orbital is large compared to the spin-orbit interaction. The interaction of 5d with the neighboring anion ligands (the crystal field interaction) degenerate 5d levels of the free ion and shifts the whole 5d configuration (centroid shift) toward lower energy. The 5d splitting depends on the site symmetry. Both the crystal field splitting and the centroid shift lowers the lowest 5d level, which is known as the redshift or depression D [12]. The value of D determines the emission color and excitation wavelength of the 4f-5d transitions. A good example of 4f-5d transition is related to the Ce^{3+} ion. The ground state of Ce^{3+} ion consists of an optically active electron in the 4f shell. Its 5d excited state is strongly affected by the crystal

environment. The crystal environment can split the 5d level by as much as 25000 cm^{-1} depending on the host material. In SrF_2, Ce^{3+} emits broadband emission centered at 330 nm that originating from 5d-4f

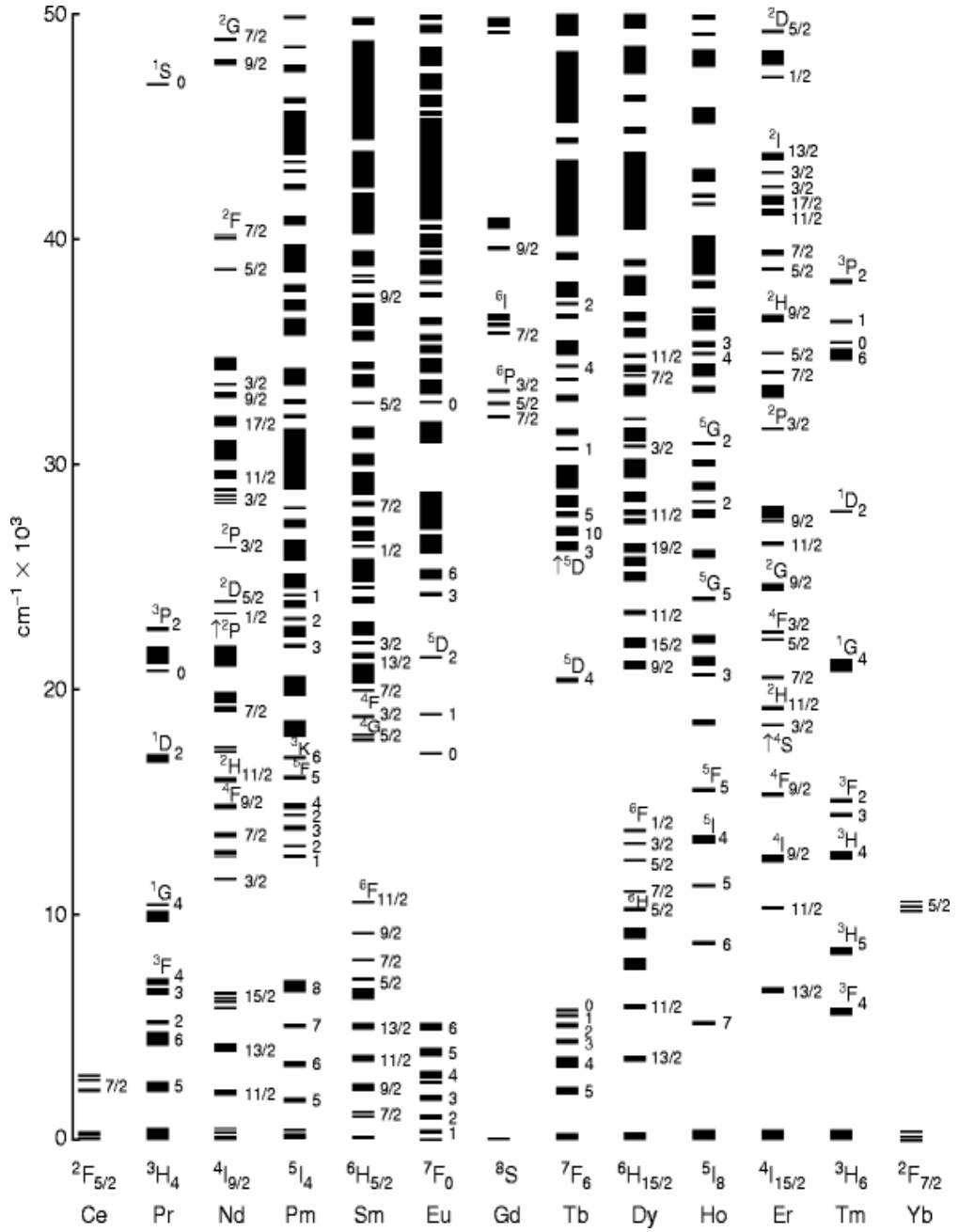

transition.

Fig. 2.7: Dieke diagram for energy-levels of Ln^{3+} ions [11].

2.4 Cerium (Ce^{3+})

Cerium is one of the most of fascinating elements in the periodic table and continues to attract a lot of attention. Its most remarkable about Ce^{3+} was that his transition that originates from one localized 4f electron, to a tetravalent metallic state, comparable to titanium or zirconium. The idea was that the localized 4f electron in trivalent cerium becomes promoted to the conduction band. This promotion model provides a satisfactory explanation of the drastic volume collapse, since four valence electrons bind considerably stronger than just three [2].

However, it was later demonstrated that the energy difference between these two metal valence states in cerium is large, of the order of 2 eV, completely invalidating this conventional valence change picture for the transition. Similarly, when more sophisticated experimental tools were made available for studies at high pressure, it became increasingly clear that there is no dramatic change in the electron occupation of the 4f orbital across the volume collapse region. Since then many spectroscopic investigations have been directed to the cerium problem [6].

Early on it was proposed that the pressure induced collapse was due to a fundamental change of the character the 4f state. On the low density side the 4f electron is localized, forms an atomic-like magnetic state and does not contribute to the interatomic bonding. In the high density phase the 4f electron is instead itinerant, metallic, and contributes significantly to the bonding causing the volume collapse. This metallization of the 4f-electron means that this phase transformation can be viewed upon as a Mott transition regarding the 4f behavior [6].

The free-ion configuration of cerium consists of xenon-like core with 54 electrons and a valence shell containing one 4f electron. This is

further split into two $^2F_{7/2}$ and $^2F_{5/2}$ spin levels. The excited 5d levels are also split into the $^2D_{3/2}$ and $^2D_{5/2}$ energy levels due to spin-orbit interactions. However, when the cerium ions are embedded in a host matrix, the energy level configuration changes considerably. The crystal field tends to split the excited 5d levels in cerium into 4 to 5 separate energy levels, [4].

CHAPTER THREE

EXPERIMENTAL AND CHARACTERIZATION TECHNIQUES

3.1 Experimental Procedure

For the co-precipitation process, analytical grade of $Sr(NO_3)_2$, $Ca(NO_3)_2.6H_2O$, $Ce(NO_3)_3.6H_2O$ and NH_4F were used without further purification. Sodium hydroxide was used to adjust the pH of the system, which were 8.5 in this study. For a typical synthesis of the mixed fluoride 30 mmol of NH_4F and 0.1 mol/mL of sodium hydroxide were added drop-wise to an aqueous solution containing $Sr(NO_3)_2$, $Ca(NO_3)_2.6H_2O$ and $Ce(NO_3)_3.6H_2O$ in a period of about 30 min. After one hour of stirring, the mixture was left for 5 hours. Then the product was collected by using a centrifugal and washed with water and ethanol. Finally, the product was dried for 48 hours in an oven at 80 ^{0}C. Then the structural and luminescent properties of the samples were studied by using – ray diffraction and Photoluminescence techniques.

3.2 X-Ray Diffraction (XRD)

X-ray diffraction (XRD) is a powerful nondestructive technique for characterizing crystalline materials. It provides information on structures, phases, preferred crystal orientations (texture), and other structural parameters, such as average grain size, crystallinity, strain, and crystal defects. X-ray diffraction peaks are produced by constructive interference of a monochromatic beam of X-rays scattered at specific angles from each set of lattice planes in a sample. The peak intensities are determined by the distribution of atoms within the lattice.

Consequently, the x-ray diffraction pattern is the fingerprint of periodic atomic arrangements in a given material.

Discovered the crystalline substances act as three-dimensional diffraction gratings for X-ray wavelengths similar to the spacing of planes in a crystal [13].

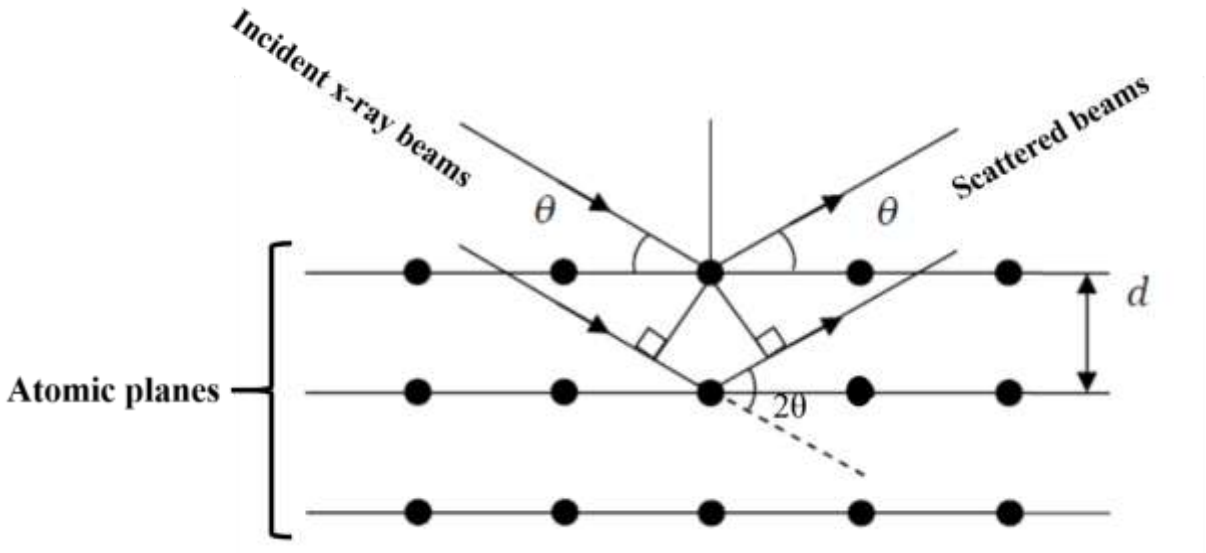

Fig. 3.4: Sketch of Bragg's law and scattering from atoms.

X-ray diffraction is now a common technique for the study of crystal structures and atomic spacing. x-ray diffraction is based on constructive interference of monochromatic x-rays and a crystalline sample, figure 3.1. These x-rays are generated by a cathode ray tube, filtered to produce monochromatic radiation, collimated to concentrate, and directed toward the sample (Figure 3.2).

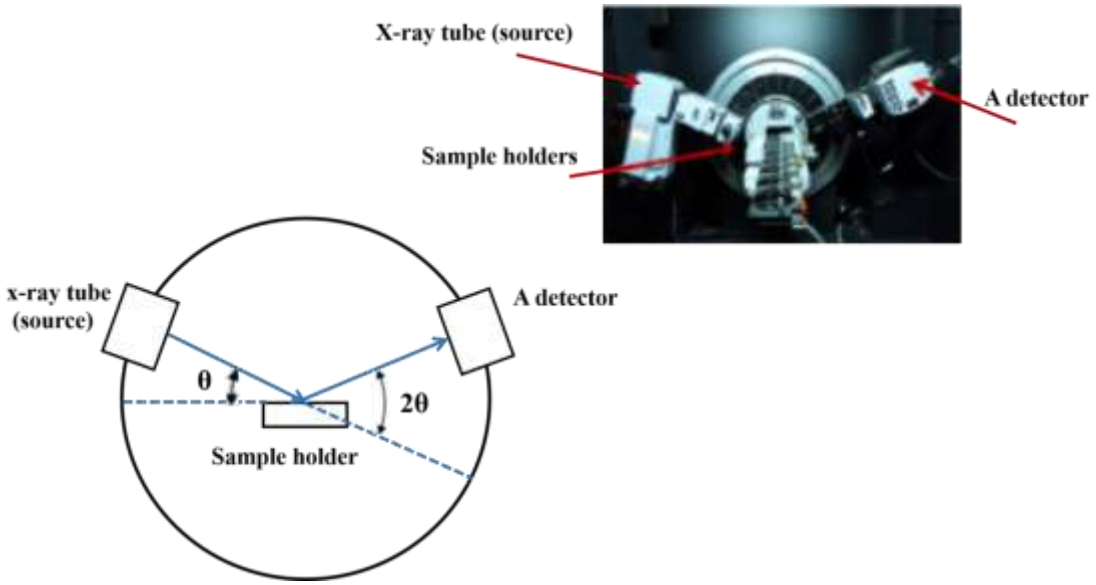

Fig. 3.2: Sketch of x-ray diffract meter. The photo is for Broker AXS D8 advance x-ray diffract meter.

The interaction of the incident rays with the sample produces constructive interference (and a diffracted ray) when conditions satisfy Bragg's law:

$$n\lambda = 2d\sin(\theta)$$

where n is an integer, λ is the wavelength of the x-rays (0.154 nm), d is the interplanar spacing generating the diffraction, and θ is the diffraction angle. This law relates the wavelength of electromagnetic radiation to the diffraction angle and the lattice spacing in a crystalline sample. These diffracted X-rays are then detected, processed, and counted. By scanning the sample through a range of 2 θ angles, all possible diffraction directions of the lattice should be attained due to the random orientation of the powdered material. Conversion of the diffraction peaks to d-spacings allows identification of the compound because each compound has a set of unique d-spacings. Typically, this is achieved by comparison of d-spacings with standard reference patterns.

X-ray diffractometers consist of three basic elements: an X-ray tube, a sample holder, and an X-ray detector (figure 3.1). X-rays are generated in a cathode ray tube by heating a filament to produce electrons, accelerating

the electrons toward a target by applying a voltage, and bombarding the target material with electrons. When electrons have sufficient energy to dislodge inner shell electrons of the target material, characteristic x-ray spectra are produced. These spectra consist of several components, the most common being K_a and K_b. K_a consists, in part, of K_{a1} and K_{a2}. K_{a1} has a slightly shorter wavelength and twice the intensity of K_{a2}. The specific wavelengths are characteristic of the target material (Cu, Fe, Mo, Cr). Filtering, by foils or crystal monochrometers, is required to produce monochromatic X-rays needed for diffraction. K_{a1} and K_{a2} are sufficiently close in wavelength such that a weighted average of the two is used. Copper is the most common target material for single-crystal diffraction, with CuK_a radiation $\lambda = 1.5418$ Å.

From the XRD pattern, the mean crystallite size can be calculated. The idea was first investigated by Paul Scherrer who examined the effect of limited particle size on x-ray diffraction patterns and it is known as the Scherrer's equation [14],

$S = K\lambda/\beta\cos(\theta)$

where S is the mean cystallite size, which may be smaller or equal to the grain size, K is the shape factor, β is the line broadening at half the maximum intensity (FWHM) in radians and θ is the Bragg's angle.

The XRD data of this study were collected by using a Bruker D8 Advance diffractometer equipped with a copper anode of x-ray tube (λ = 0.154 nm), operating at a voltage of 40 KV and a current of 40 mA. Moreover, the Nickel was used as a filter for monochromatic x-rays to absorb the x-ray waves under 0.154 nm wavelength.

3.3 Photoluminescence spectroscopy (PL)

PL spectroscopy is a technique capable of measuring the emission and excitation as well as the luminescence lifetime of a luminescent material. In this technique, the light photons normally used as excitation source. Photoluminescence spectroscopy measurements divided into two domains, steady-state and time-resolved PL. In steady-state PL, the information normally extracted from the emission and excitation spectra, while in time-resolved measurements the decay curve is of interest. A typical PL spectrum is a distribution of the emission intensity as a function of wavelength measured at fixed excitation wavelength. A photoluminescence excitation spectrum is a measure of emission intensity at a single emission wavelength as a function of excitation wavelength. The photoluminescence excitation spectrum to a good approximation is identical to the absorption spectrum if there is no multiple overlapping excited states occurred [15].

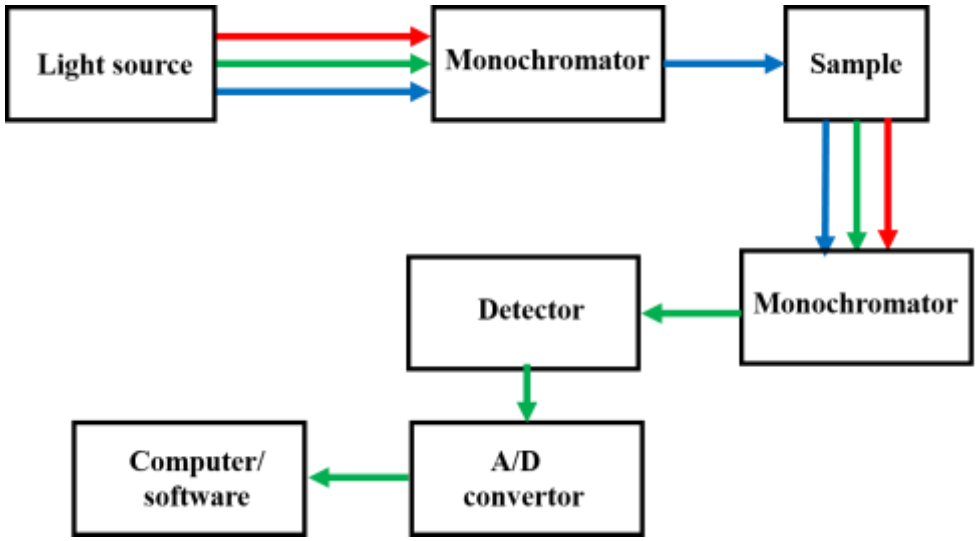

Fig. 3.2: Schematic illustration of basic components of a spectrofluorometer.

Fig. 3.2 schematically shows the basic components of PL spectrofluoremeter. In a typical PL measurement, the light photons that generated by the source enter into a monochromator, which selectively

transmit a specific excitation wavelength that used to excite the sample. The emitted light from the sample is directed by lenses, dispersed by another monochromator, then collected by detector, i.e. PMT, photodiodes or CCD. The analog to digital convertor converts the electrical signal that generated by the photo detector into a digital signal. The digital signal then processed by software on a computer [15]. In this study, Edinburg instrument Fs980 system was used to collect our PL data. It is equipped with PMT detector and a xenon lamp that exhibits a wide excitation spectrum range between 200 and 1100 nm. The monochromator generally produced good monochromatic light.

While the photoluminescence is a sensitive technique to study the optical properties of the materials, better chemical and physical information can be obtained from the same technique by using the time-dependent nature of the photoluminescence [15]. A pulsed excitation source and a fast detector are required in time-resolved photoluminescence measurements. Nowadays, lifetime as short as 10 femtoseconds can readily be detected. Time-resolved photoluminescence provides better information on the chemical surrounding of the material. Therefore, time-resolved measurements can be used to investigate the energy transfer and dynamic quenching that can occur on the system [15]. The time-resolved instrument is basically the same as the photoluminescence measurements [15]. The only difference is that in time-resolved instrument a pulsed source is included instead of continuous light source. The luminescence decay curves on this study were recorded under pulsed excitation (HORIBA scientific) with NanoLED diode and pulsed excitation using a diode pumped YAG laser with a 335 nm excitation wavelength, power of 1.3 milliwatt and a SR430 Multichannel scaler photomultiplier.

CHAPTER FOUR

RESULTS AND DISCUSSION

4.1 X-ray analysis

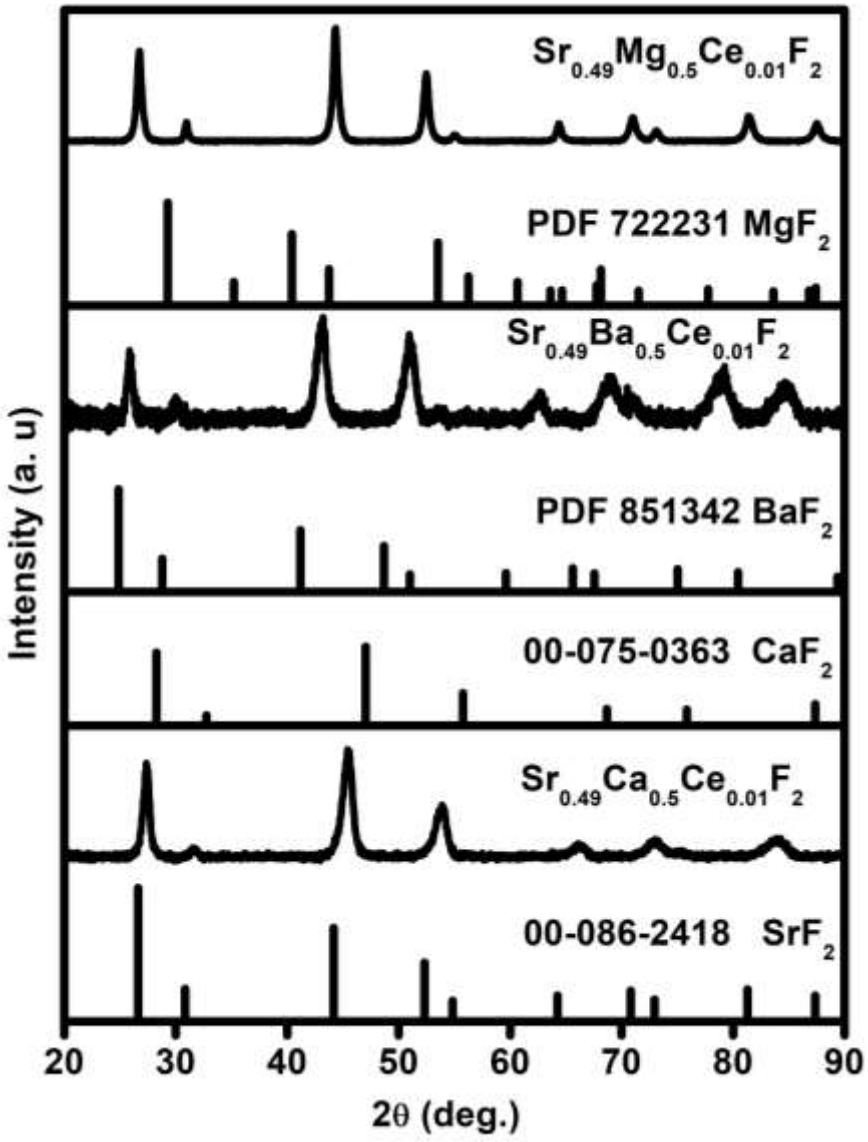

Figure 4.1. XRD pattern of $Sr_{0.49}M_{0.5}Ce_{0.01}F_2$ (M = Ca, Ba and Mg) with standard data of SrF_2, BaF_2, MgF_2 and CaF_2 for comparison.

Figure 4.1 shows the XRD pattern of $Sr_{0.49}M_{0.5}Ce_{0.01}F_2$ (M = Ca, Ba and Mg)as well as the standard data of SrF_2, BaF_2, MgF_2 and CaF_2 for comparison. The strong diffraction peaks indicate that the samples

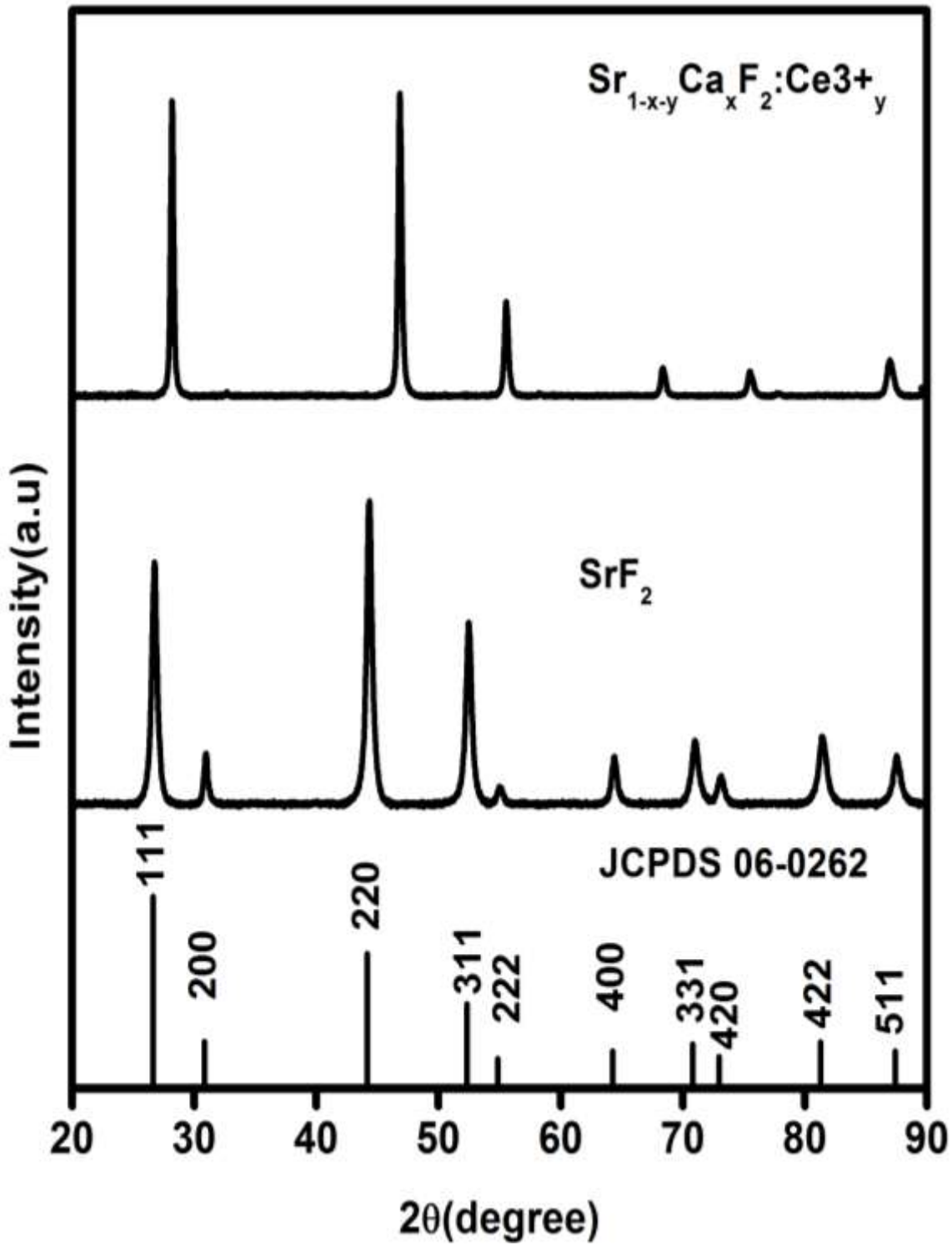

The estimated average crystallite size (**S)** for pure and mixed fluoride materials is calculated by using the diffraction peaks and Scherrer' s equation.. The average crystallite size of the pure SrF_2 was found to be 7.6 nm. The average crystallite size mixed sample with highly Ca, Ba and Mg ions concentration was increased due to the mixer formation.

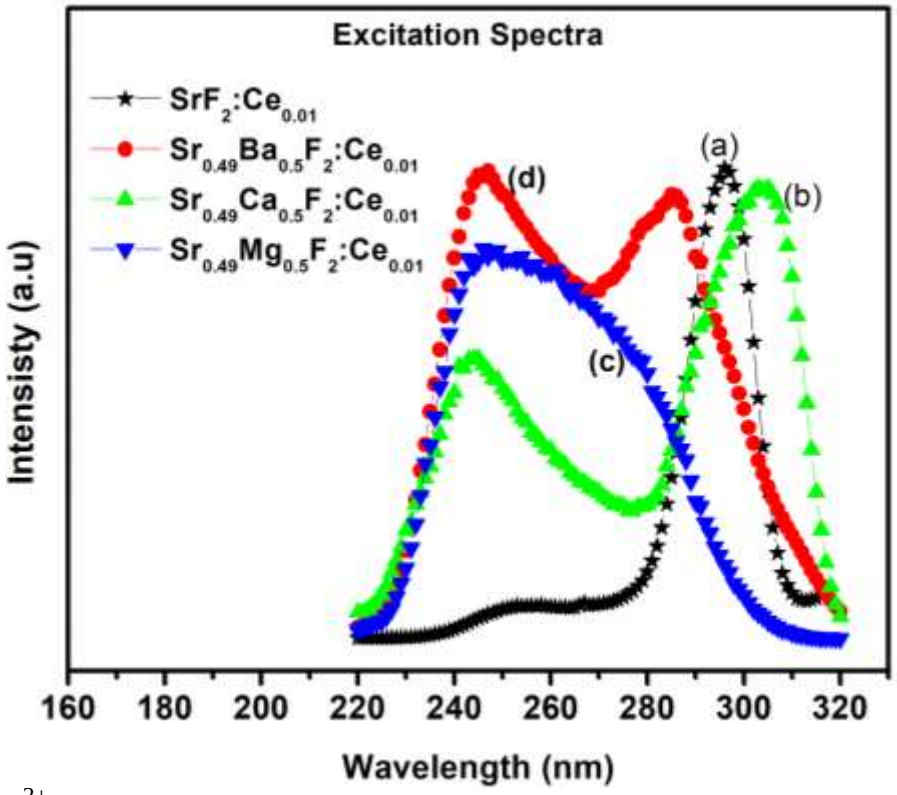

Figure 4.3: Ce^{3+} (1 mol%) excitation in $Sr_{0.49}M_{0.5}Ce_{0.01}F_2$ (M = Ca, Ba and Mg). (a) Excitation for 327 nm emission in $SrF_2:Ce_{0.01}$. (b) Excitation for 336 nm emission in $Sr_{0.49}Ca_{0.5}F_2:Ce_{0.01}$. (c) Excitation for 328 nm emission in $Sr_{0.49}Mg_{0.5}F_2:Ce_{0.01}$. (d) Excitation for 340 nm emission in $Sr_{0.49}Ba_{0.5}F_2:Ce_{0.01}$.

The excitation spectra of the Ce^{3+} doped mixed fluoride materials are shown in figure 4.2. Curve a shows the excitation spectrum of the $SrF_2:Ce^{3+}{}_{0.01}$ sample. The excitation spectrum of Ce doped SrF_2, monitored at λ_{exc}= 327 nm, consists of two peaks. The prominent peak is centred at 295 nm and the less intense peak centred at 250 nm. The bands centered at 295 nm and 250 nm

corresponds to the transitions from the ground state, $^2F_{5/2}$, of Ce^{3+} (4f) to the different components of the excited Ce^{3+} 5d states [16]. Curves b-d show the effect of the mixed fluoride on the excitation. Partial substitution of Sr^{2+} by Ba^{2+}, Ca^{2+} and Mg^{2+} ions produced entirely different results. Mg^{2+} substitution results in only one broad excitation

peak centered at 240 nm, curve c. The excitation peak around 250 nm becomes more prominent by the substitution of Sr^{2+} by Ba^{2+} ions. Substitution by Ca shifts the excitation peak of 295 nm to higher wavelength and the peak around 250 nm to lower wavelength. Relative intensities of the components at the shorter wavelengths increases.

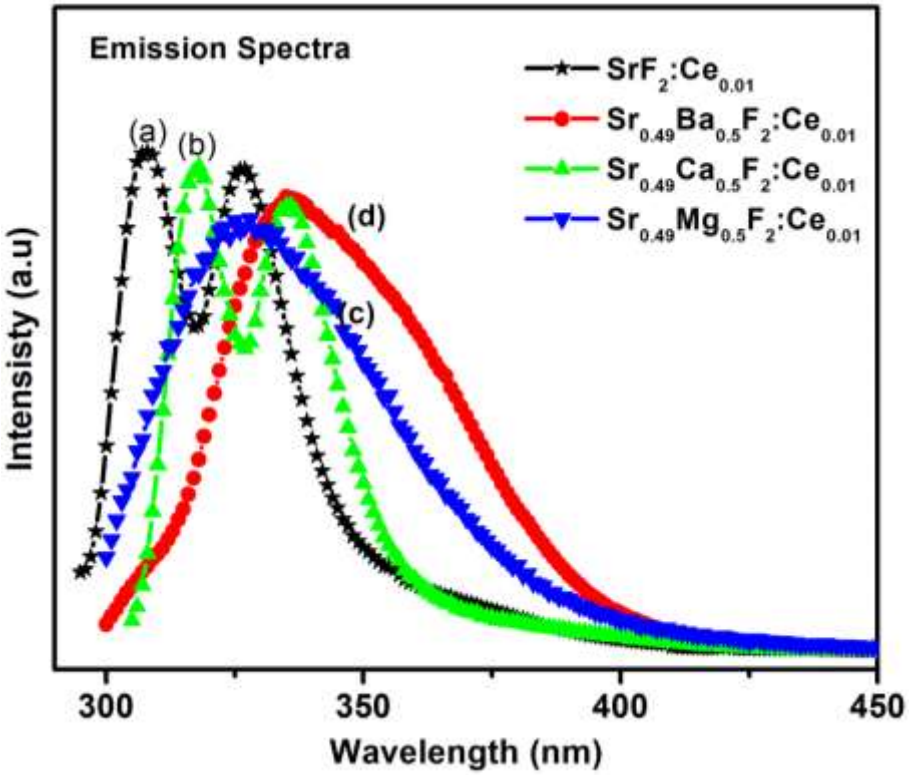

Figure 4.3. Ce^{3+} (1 mol%) emission in $Sr_{0.49}M_{0.5}Ce_{0.01}F_2$ (M = Ca, Ba and Mg). (a) Emission in $SrF_2:Ce_{0.01}$ for 295 nm excitation. (b) Emission in $Sr_{0.49}Ca_{0.5}F_2:Ce_{0.01}$ for 305 nm excitation. (c) Emission in $Sr_{0.49}Mg_{0.5}F_2:Ce_{0.01}$ for 250 nm excitation. (d) Emission in $Sr_{0.49}Ba_{0.5}F_2:Ce_{0.01}$ for 285 nm excitation.

Figure 4.3 shows the PL spectra for $Sr_{0.49}M_{0.5}Ce_{0.01}F_2$ (M = Ca, Ba and Mg). In $SrF_2:Ce_{0.01}$ emission, curve a, two bands are observed at 308 nm and 327 nm upon excitation into the 295 nm band. These emission bands correspond to the parity allowed transition of the lowest component of the excited state $^2D_{3/2}$ to the split ground state into their $^2F_{5/2}$ and $^2F_{7/2}$ components, which is in good agreement with previous studies [16, 17]. The structure of SrF_2 can be regarded as a simple cubic array of touching F ions with every second void occupied by a Sr^{2+} ion. When a Sr^{2+} ion is

substituted by a trivalent lanthanide ion, charge balance compensating F ions enter the fluoride structure leading to dominant defect structures. At low concentration the additional F ion goes into the next-nearest-neighbor void of the trivalent lanthanide ion giving isolated tetragonal (C_{4V}), trigonal (C_{3V}) and rhombic (C_{2V}) defects [18, 19]. Charge-compensating interstitial F ions can modify the geometry and the constitution of the centre by taking a position close to the lanthanide ion. Perturbations of trigonal and tetragonal symmetries induced by a F ion are usually observed in trivalent lanthanide ions doped SrF_2. However, in this case the cubic crystal field is not perturbed as the F ion is away from the lanthanide ion [20]. M^{2+} cations can also substitute Sr^{2+} ions without any need for charge compensation. When Sr^{2+} is substituted by Ca^{2+} in the $Sr_{0.49}Ca_{0.5}Ce0.01F_2$ sample, the emission maximum shifts to longer wavelengths and the excitation spectrum bands at shorter wavelengths becomes more prominent (figure 3, curve b). The stark shift does not change much with Ca^{2+} substitution. Emission of Ce^{3+} in SrF_2 and $Sr_{0.49}Ca_{0.5}Ce_{0.01}F_2$ is thus characteristic of these configurations.

Modifications in the PL spectra were produced by Ba and Mg dopants. A prominent shift in the emission spectrum for substitution by Mg atoms was observed in curve c. The shape of the emission band also changed dramatically with a marginal increase in the width. The spectrum showed only one broad band centered at 328 nm. The half-width of the emission band was about 43 nm. The same behavior was observed by La substitution but the peak was blue shifted. The incorporation of Ba, curve d, also resulted in a significant change in the Ce^{3+} spectra. Ce^{3+} in $Sr_{0.49}Ba_{0.5}Ce_{0.01}F_2$ exhibited a broad emission band that was centered at 340 nm. The half-width of the emission band was about 48 nm. There was also asymmetric broadening of the emission band at 375 nm. The shift was quite large compared with that of $Sr_{0.49}Mg_{0.5}Ce_{0.01}F_2$ therefore

the maximum shift to longer wavelength was observed at the $Sr_{0.49}Ba_{0.5}Ce_{0.01}F_2$ sample.

We further studied the modification of the Ce^{3+} doped SrF_2-based materials by analysing the decay curves for the Ce^{3+} ions with different cations substitution. The luminescence decay curves of Ce^{3+} doped various SrF_2-based materials are shown in figure 4.4. The luminescence decay curve of Ce^{3+} doped SrF_2 possesses the longest lifetime. The incorporation of Ca^{2+} ions resulted in small change in the Ce^{3+} decay curve. The noticeable change in the Ce^{3+} decay curve is observed in the SrF_2-BaF_2 based sample. The decrease in the Ce^{3+} lifetime in Ba substitution is attributed to the crystal field environment around Ce^{3+}, which is the Ba atom. This lifetime agreed well with that of BaF_2 crystal [21].

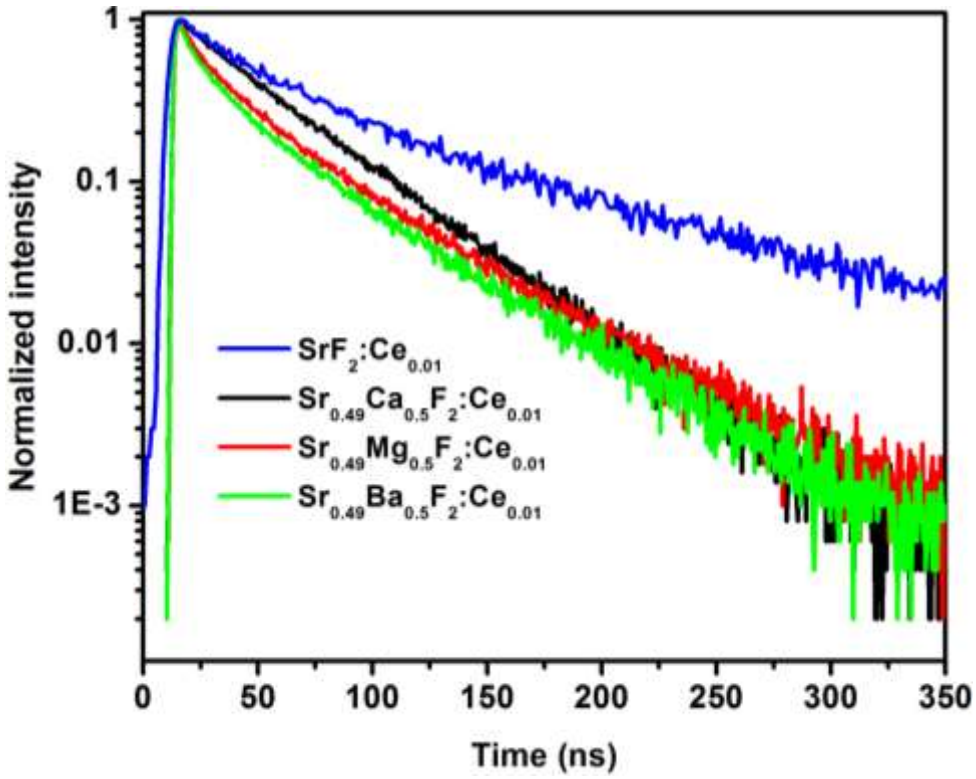

Figure 4.4. Decay curves of Ce^{3+} 5d in $Sr_{0.49}M_{0.5}Ce_{0.01}F_2$ (M = Ca, Ba and Mg).

CHAPTER FIVE
CONCLUSIONS

It is therefore seen that both the excitation and emission spectra of $SrF_2:Ce^{3+}$ can be modified by various types of substitutions. For the optimum sensitization, the emission band of the Ce^{3+} ion should overlap with the Ln^{3+} ions. Thus, efficient energy transfer between a sensitizer and a donor can only occur when the emission band of the sensitizer overlap with the excitation band of the donor. Ce^{3+} doped $Sr_{1-x}M_xF_2$ (where M is Ca, Ba, Mg and La) exhibited emission in the range of 300 nm to 375 nm. Modification in the emission spectrum in $Sr_{0.49}Ba_{0.5}Ce_{0.01}F_2$ is of interest. The position of the Ce^{3+} peak upon Ba substitution can be suitable for some 4f-4f lanthanide ions for better sensitization. A major problem limiting the conversion efficiency of photovoltaic cells is their insensitivity to a full solar spectrum. The spectral distribution of sunlight at Air Mass 1.5 global (AM 1.5G) consists of photons with wide wavelengths ranging from ultraviolet to infrared (280– 2500 nm, 0.5– 4.4 eV). A downconversion layer can convert the high energy photons, about 300 nm to 500 nm, into two NIR photons that can be utilized by c-Si solar cell. A noticeable modification was however also achieved in the excitation spectrum of $Sr_{0.49}Ba_{0.5}Ce_{0.01}F_2$. The spectrum shifted to shorter wavelengths (around 245 nm) that is far from the spectral distribution of sunlight at AM 1.5G.

These results are therefore not suitable for solar cell applications.

References

[1] D. Timmerman, I. Izeddin, P. Stallinga, I. N. Yassievich and T. Gregorkiewicz, Nat. Photonics, 2 (2008) 105-108.

[2] R. D. Schaller, V. M. Agranovich, V. I. Klimov, Nat. Phys. 1 (2005) 189-195.

[3] Judd-Ofelt theory: principles and practices. Available from http://link.springer.com/chapter/10.1007/1-4020-4789-4-21page-1, (Accessed on 19.3.2020).

[4] B. M. Van der Ende, L. Aarts, A. Meijerink, Phys. Chem. Chem. Phys. **11** (2009) 11081-11095.

[5] R. Shendrik, E. A. Radzhabov, A. I. Nepomnyashchikh, Radiat. Meas. **56** (2013**)** 58-61.

[6] X. Huang, S. Han, W. Huang, X. Liu, Chem. Soc. Rev. 42 (2013) 173-201.

[7] Strontium Fluoride. Available from http://www.americanelements.com/srf.html, (Accessed on 25.02.2020).

[8] F. T. Charnock, Dynamic of Dipolar Defect in Rare Earth Doped Alkaline-Earth Fluoride Crystal, Wake Forest University, PhD Thesis, (1999).

[9] Judd-Ofelt theory: principles and practices. Available from http://link.springer.com/chapter/10.1007/1-4020-4789-4-21page-1, (Accessed on 19.12.2019).

[10] G. H. Dieke and H. M. Crosswhite, Appl. Opt. 2 (1963) 675-686.

[11] A. Shalav, Rare-Earth Doped Up-converting Phosphors For an Enhanced Silicon Solar Cell Response, University of New South Wales, PhD Thesis, (2006).

[12] J. G. Sole', L. E. Bausa, D. Jaque, An Introduction to the Optical Spectroscopy of Inorganic Solids, John Wiley and Sons Ltd, England, (2005).

[13] Basics of X-ray di_raction. Available online from http://old.vscht.cz/clab/RTG/dokumenty/thermo/xrd/Introduction%20to%20powder%20di_raction.pdf (Accessed 06.03.2020).

[14] C. Oprea, V. Ciupina, G. Prodan, Romanian J. Phys. 53 (2008) 223-230.

[15] J. Z. Zhang, Optical Properties and Spectroscopy of nanomaterials, Wold Scientific, Singapore, (2009).

[16] M. Y. A. Yagoub, H. C. Swart, L. L. Noto, P. Bergman, E. Coetsee, Materials **8** (2015) 2361-2375.

[17] V. S. Singh, C. P. Joshi, S. V. Moharil, P. L. Muthal, S. M. Dhopte, Lumin. **30** (2015) 1101– 1105.

[18] J. A. Campbell, J. P. Laval, M. T. Fernandez-Diaz, M. Foster, J. Alloys. Compd. **111** (2001) 323– 324.

[19] S. S. Pote, C. P. Joshi, S. V. Moharil, P. L. Muthal, S. M. Dhopte, J. Lumin. **130** (2010) 666– 668.

[20] M. Bouffard, J. P. Jouart, M. F. Joubert, Opt. Mater. **14** (2000) 73-79.

[22] S. Kh. Batygov, L. S. Bolyasnikova, V. A. Demidenko, E. M. Garibin, M. E. Doroshenko, K. V. Dukelskioe, A. A. Luginina, I. A. Mironov, V. V. Osiko, P. P. Fedorov, Doklady phys. **422** (2008) 179– 181.